External Grant Award Number 05HQGR0041

INTEGRATING GEOLOGIC, PALEOSEISMIC, AND GEODETIC DATA USING A BAYESIAN MODELING APPROACH TO CONSTRAIN FAULT-ZONE AND LOWER-CRUSTAL RHEOLOGY ALONG THE SOUTHERN SAN ANDREAS FAULT, CA

Roland Bürgmann P.I., with Kaj M. Johnson and George E. Hilley
Department of Earth and Planetary Sciences
University of California, Berkeley
307 McCone Hall
Berkeley, CA 94720-4767
Tel: (510)643-9545; FAX:510)643-9980; burgmann@seismo.berkeley.edu
URL: http://www.seismo.berkeley.edu/∼burgmann

External Grant Award Number 05HQGR0041

INTEGRATING GEOLOGIC, PALEOSEISMIC, AND GEODETIC DATA USING A BAYESIAN MODELING APPROACH TO CONSTRAIN FAULT-ZONE AND LOWER-CRUSTAL RHEOLOGY ALONG THE SOUTHERN SAN ANDREAS FAULT, CA

Roland Bürgmann P.I., with Kaj M. Johnson and George E. Hilley
Department of Earth and Planetary Sciences
University of California, Berkeley
307 McCone Hall
Berkeley, CA 94720-4767
Tel: (510)643-9545; FAX:510)643-9980; burgmann@seismo.berkeley.edu
URL: http://www.seismo.berkeley.edu/∼burgmann

1 Abstract

In this project we used geologic and paleoseismic data as a priori knowledge in a Bayesian model that relates lower crustal and upper mantle properties to deformation observed geodetically during the earthquake cycle. We simultaneously estimated fault slip rates and lithosphere viscosity structure in the Mojave region of the San Andreas fault system. We developed a multi-layered earthquake cycle model consisting of an elastic crust overlying viscoelastic layers representing the lower crust, uppermost mantle and upper mantle. The relative abundance of geodetic and paleoseismic data in the Mojave region makes this an ideal location to resolve slip rate and viscosity structure. We used GPS measurements of postseismic relaxation following the 1992 Landers earthquake, triangulation measurements spanning 1932-1977, GPS measurements of the contemporary velocity field, and paleoseismic data along the San Andreas fault to invert for viscosity structure in the Mojave regions and slip history of the San Andreas fault. We find that the lower crust, from 15-30 km depth, has viscosity of 1019-1020 Pa s, the uppermost mantle from 30-60 km has viscosity of 1020-1022 Pa s, and the underlying upper mantle has viscosity of 1018-1019 Pa s. This is consistent with inferences from laboratory experiments of a relatively high viscosity upper mantle and lower viscosity lower crust. We find a 24-32 mm/yr slip rate on the Mojave segment of the San Andreas fault, in agreement with geologic estimates.

2 Introduction

A challenge for imaging lithosphere viscosity structure in actively deforming regions is that the current deformation field is a function of fault slip history and viscosity structure. *Savage and Prescott* [1978] demonstrated this with an earthquake cycle model consisting of a fault with periodic, sudden slip events in an elastic crust overlying a viscoelastic lower crust and mantle. In this model, the surface velocity field depends on the fault slip rate,

the thickness of the elastic crust, the time since the last earthquake, the average repeat time of earthquakes, and the viscosity below the elastic crust. As an illustration of this, we cite the study of *Dixon* et al. [2003] who show that estimates of slip rate in the Owens Valley fault zone in eastern California can vary by as much as a factor of three, depending on the choice of asthenosphere viscosity. *Dixon* et al. [2003] showed that elastic block models, which implicitly assume relaxation times greater than the average recurrence interval of earthquakes, predict higher slip rates using geodetic data than estimated from geologic data, while viscoelastic earthquake cycle models with asthenosphere relaxation times less than the average recurrence interval predict slip rates similar to those estimated from geological data.

There is a similar discrepancy between slip rates estimated with geodetic and geologic data for the Mojave region of the San Andreas fault. According to geologic estimates, the San Andreas fault slips 25-35 mm/yr along this segment (*Sieh and Jahns* [1984]) while elastic block models predict lower slip rates of about 15 mm/yr (*Becker* et al. [2004], *Meade and Hager* [2005]). In this research we try to resolve this discrepancy through a simultaneous inversion for fault slip rate and lithosphere viscosity structure using an extended version of the *Savage and Prescott* [1978] model. We construct a model consisting of multiple viscoelastic layers that represent the lower crust, uppermost mantle, and upper mantle. We identify the viscosity structure of the lithosphere and the slip history on the San Andreas fault that is consistent with geodetic measurements of surface deformation, paleoseismic data on timing of past earthquakes, geologic estimates of fault slip rates, and inferences of relaxation times associated with isostatic adjustments.

The average lower crust and mantle viscosity in the western United States has been inferred using several different data sets. GPS measurements of contemporary surface deformation are used to infer the average viscosity with earthquake cycle models (e.g., *Segall* [2002], *Johnson and Segall* [2004b]). The mantle viscosity structure under southwest Montana has been inferred from models of viscoelastic relaxation following the 1959 Hebgen Lake earthquake constrained by historical geodetic measurements of surface deformation (*Nishimura and Thatcher* [2003]). The uplift of paleo-shorelines due to isostatic adjustments following the removal of ancient lakes in the western United States have been dated and modeled to obtain viscosity estimates (e.g., *Bills* et al. [1994]). Geodynamic models have been used to infer lower crust and mantle viscosities by modeling the long-term evolution of geologic structures and topography (e.g., *Kaufman and Royden* [1994]).

All of the studies mentioned above provide estimates of lower crust and mantle viscosity using single data sets that record deformation over different time periods. Postseismic GPS time-series record rapid relaxation processes that occur over the months and years following an earthquake. GPS data in California records decadal time-scale deformation processes associated with an earthquake cycle. The paleo-lake shoreline data records relaxation processes that take place over thousands of years. It is difficult to compare or integrate results from studies examining deformation over different time periods. A motivation of the current study is to integrate various data sources covering a broad range of time periods and identify a model of the lithosphere viscosity structure that is consistent with the multiple data sets. The Mojave region is ideal for this study because of the abundance of geodetic and paleoseismic data. We have GPS time-series data of

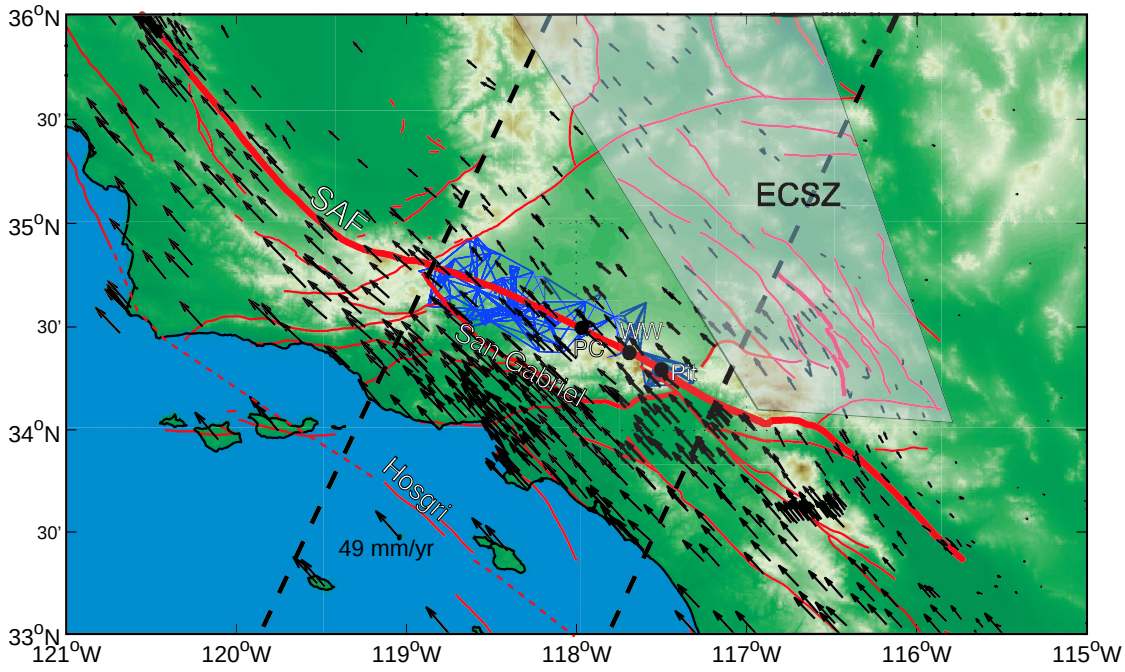

Figure 1: Location map of study area showing distribution of geodetic data and locations of paleoseismic excavation sites along the San Andreas fault. GPS velocities relative to North America. Blue mesh shows triangulation network within 10 km of the San Andreas fault. GPS data within dashed lines are used in this study. The Eastern California Shear Zone (ECSZ) is outlined with the gray box. Paleoseismic sites: PC - Pallett Creek, WW - Wrightwood, PT - Pitman Canyon.

postseismic relaxation following the 1992 Landers and 1999 Hector Mine earthquakes in the Mojave desert, triangulation data spanning 1932-1977, and GPS measurements of the contemporary velocity field (Figure 1). In addition, a detailed history of past earthquakes is beginning to emerge (Figure 2) with continued analysis of paleoseismic excavations along the San Andreas fault (*Weldon* et al. [2004], *Hilley and Young* [2006]).

3 Lithosphere rheology

While our understanding of the viscosity structure of the lithosphere in the western United States is being refined with continuing geodetic studies, several studies lead to contradictory conclusions regarding the relative viscosities of the lower crust and mantle. Table 1 summarizes viscosity estimates for the western United States. Estimates of lower crust and mantle viscosity vary over three orders of magnitude.

Laboratory creep experiments of lower crustal and upper mantle materials (e.g., *Kohlstedt* et al. [1995]) has led some to suspect that the viscosity of the lower crust is lower than the viscosity of the underlying mantle. In the western United States there is evidence to support this hypothesis and other evidence to refute it. *Deng* et al. [1998] inferred flow in the lower crust with a low viscosity of 10^{18} Pa s in the Mojave desert following the 1992 Landers earthquake, consistent with results from a geodynamic model of deformation in the eastern Mojave region (*Kaufman and Royden* [1994]). *Bokelmann and Beroza* [2000] also infer a relatively low viscosity ($< 10^{19}$ Pa s) lower crust below the

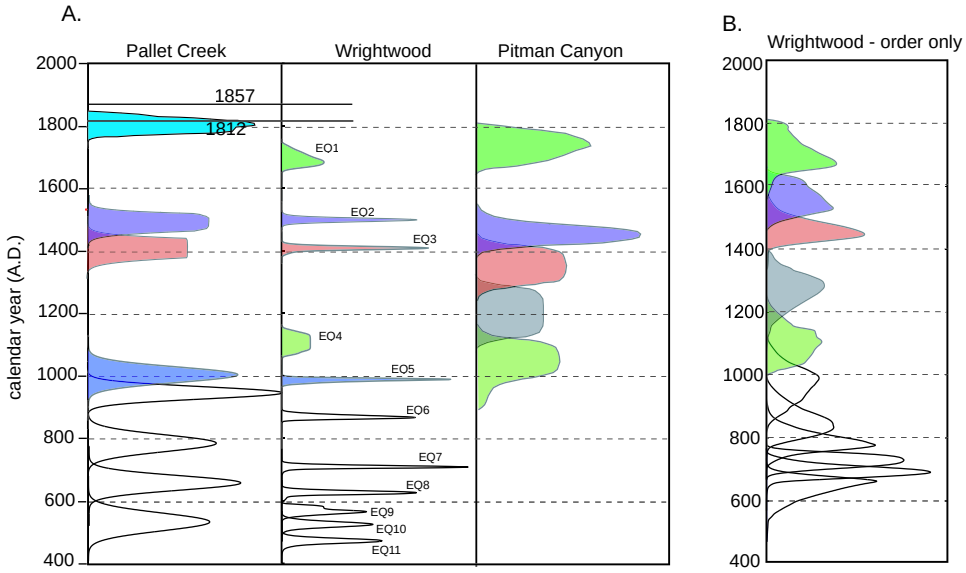

Figure 2: Probability distributions for timing of past earthquakes at the three sites labelled in Figure 1 (from *Hilley and Young* [2006]). Events that correlate in time are shaded with the same color for all three sites.

Table 1: Summary of viscosity estimates

reference	lower crust	uppermost mantle	upper mantle	data type	location
[1] *Bills* et al. [1994]	-	$5-30\times10^{19}$	$2-4\times10^{19}$	shoreline	Lake Boneville, Utah
[2] *Bills* et al. [1994]	-	3×10^{17}	$0.4-20\times10^{19}$	shoreline	Lake Bonneville, Utah
[3] *Kaufmann and Amelung* [2000]	-	$0.6-4\times10^{18}$	$2-6\times10^{17}$	leveling	Lake Meade, Nevada
[4] *Nishimura and Thatcher* [2003]	$\geq10^{20}$	$1-10\times10^{18}$	-	leveling	SW Montana
[5] *Pollitz* et al. [2000]	$8-24\times10^{18}$	$4-12\times10^{18}$	$1-6\times10^{18}$	GPS and InSAR	Landers, Mojave Desert
[6] *Pollitz* [2003]	10^{20}	5×10^{18}	-	GPS	Hector Mine, Mojave Desert
[7] *Segall* [2002]	-	-	$1-10\times10^{19}$	GPS	central California
[8] *Johnson and Segall* [2004b]	-	-	$1-30\times10^{19}$	GPS	central California
[9] *Kaufman and Royden* [1994]	10^{18}	-	-	geomorphology	eastern California
[10] *Bokelmann and Beroza* [2000]	$<10^{19}$	-	-	focal mechanisms	central California
[11] *Deng* et al. [1998]	10^{18}	-	-	GPS	Landers earthquake

1. Model assumes viscosity strictly decreases with depth. 2. Model does not assume viscosity strictly decreases with depth. 3. Measure subsidence due to filling of Lake Meade. 4. Postseismic deformation following 1959 Lake Hegben earthquake (1959 to 1987). 5. Multilayered model of Landers postseismic deformation. 6. Assumes biviscous mantle. 7. Savage-Prescott viscoelastic cycle model of interseismic velocity field. 8. Earthquake cycle model with creep in deep fault zone. 9. Analytical model of channel flow. 10. Orientations of P-T focal mechanism axes. 11. Numerical model of postseismic deformation.

San Andreas fault from focal mechanism orientations. However, *Freed and Bürgmann* [2004] and *Pollitz* et al. [2001] inferred higher viscosities in the lower crust than in the upper mantle from models of postseismic deformation following the 1992 Landers and 1999 Hector Mine earthquakes in the Mojave desert.

Studies of the average viscosity structure over decadal time scales present results that are inconsistent with estimates of average viscosity structure over longer time scales. For example, *Segall* [2002] and *Johnson and Segall* [2004b] used earthquake cycle studies to infer average mantle viscosities of $10^{19}-10^{20}$ Pa s. However, studies of transient isostatic adjustment associated with lake loads in the western United States suggest upper mantle viscosities of less than 10^{19} Pa s (*Bills* et al. [1994], *Kaufmann and Amelung* [2000], see review of results in *Dixon* et al. [2004]). This discrepancy may be due to model assumptions about viscosity structure. *Segall* [2002] and *Johnson and Segall* [2004b] assumed a uniform viscosity for the asthenosphere while *Bills* et al. [1994] and *Kaufmann and Amelung* [2000] assumed a layered viscoelastic structure.

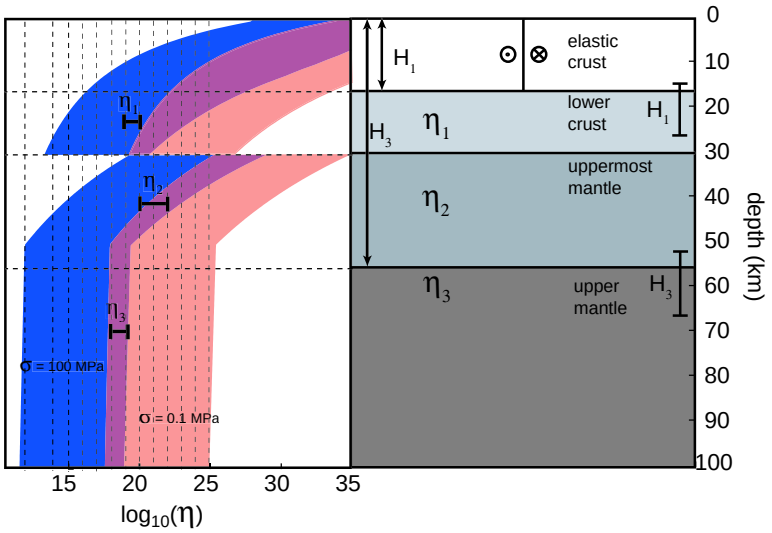

Figure 3: Theoretical viscosity distribution and geometry of multilayer viscoelastic earthquake cycle model. Rheological parameters to be solved for are viscosities of lower crust, η_1, uppermost mantle, η_2, and upper mantle, η_3 as well as depth to bottom of elastic crust, H_1, and depth to top of mantle, H_3. Theoretical viscosity profile is constructed from laboratory derived creep laws using a range of experimental values for crustal and mantle materials at two different stress levels (0.1 and 100 MPa).

Laboratory creep experiments show that lower crustal and upper mantle materials display nonlinear power-law creep behavior with effective viscosity

$$\eta = C\sigma^{(1-n)}, \tag{1}$$

where σ is differential stress, C is a material constant and is a function of temperature and activation energy, and n is typically in the range 2-4. However, by themselves, the experiments place essentially no constraints on actual effective viscosities in the lithosphere. Figure 3 shows theoretical effective viscosities for a range of shear stress values and crustal and mantle materials with varying laboratory values for C summarized in *Freed and Bürgmann* [2004]. Temperatures are assumed to decrease linearly with depth down to the top of the upper mantle. The temperature is assumed to be constant with depth in the upper mantle as evidenced by seismic inversions for temperature in the western Unite States (*Goes and van der Lee* [2002]). The hypothetical effective viscosities range over 10 orders of magnitude.

4 Earthquake history in the Mojave region

Geologic and paleoseismic studies indicate that the San Andreas fault slips 25-35 mm/yr along the Mojave segment. The remaining 15-25 mm/yr needed to keep up with the 50 mm/yr of total shift across the plate boundary is taken up on neighboring faults, mostly within the Eastern California Shear zone.

The paleoseismic record provides some detail on the earthquake history on the San Andreas fault. Estimates of earthquake timing is available from nine trenching sites along the southern and central San Andreas fault. The most complete record of past

earthquakes is recorded at the Wrightwood site on the Mojave segment were 14 events have been dated going back about 1600 years into the record (e.g., *Fumal* et al. [2002], *Weldon* et al. [2004]). *Hilley and Young* [2006] reinvestigated the paleoseismic data and calculated event probabilities using a robust Bayesian statistical method. Correlations between sites reveals a complex rupture behavior in which recurrence times and rupture lengths vary with time. *Weldon* et al. [2004] and *Hilley and Young* [2006] show that various scenarios for the segmentation of rupture on the San Andreas fault are possible given the data constraints. Because we are using 2D models, this paper is not concerned with the various rupture scenarios that might be inferred from the paleoseismic data. We will assume the rupture history is adequately characterized by data from the Wrightwood site (Figure 2), which displays the most complete record of paleo-earthquakes.

We know the exact timing of the two most recent large earthquakes on the Mojave segment of the San Andreas fault. The 1857 Fort Tejon earthquake produced slip of about 7-9 meters along the Carrizo section (*Sieh* [1978], *Liu* et al. [2004]) and 3-6 meters along the Mojave segment (*Sieh* [1978], *Salyards* et al. [9992]). *Salyards* et al. [9992] suggest that the two earthquakes before the 1857 event produced 5.5 and 6.25 meters of offset at Pallett Creek (Figure 1).

Geodetic studies indicate that about 25% of the plate motion across the diffuse Pacific/North American plate boundary occurs within the Eastern California Shear Zone. The nature and history of earthquake behavior in this zone is a topic of current research and is not very well understood. Paleoseismic data in this region is too sparse at this time to make many direct comparisons with models of geodetic data.

5 Mojave data

We show that it is necessary to have surface deformation measurements that sample multiple time periods of an earthquake cycle to resolve the lithosphere viscosity structure. In order to have the broadest temporal data coverage, we use several sources of geodetic data: 1) GPS measurements of the contemporary velocity field, 2) GPS measurements of postseismic deformation following the 1992 Landers earthquake, and 3) triangulation measurements spanning 1932 to 1977. The locations of the measurements are displayed in Figure 1.

The contemporary GPS velocity field in the Mojave region (Figure 1) is taken from the SCEC Crustal Motion Map, version 3.0 (http://epicenter.usc.edu/cmm3/). The crustal motion map is constructed based on GPS data since 1986, United States Geological survey trilateration data spanning 1970-1992, and VLBI data collected by the NASA Crustal Dynamics Program (1980-1994). GPS data within the dashed lines in Figure 1 is plotted in Figure 7 as a projection on a profile perpendicular to the San Andreas fault.

Triangulation data were obtained for the entire state of California from the National Geodetic Survey (*NGS* [2004]). We select triangulation measurements within 10 km of the San Andreas fault to estimate the average shear strain rate within a narrow zone across the fault. We calculate the shear strain rate during each time period using the method of *Frank* [1966], although as in *Thatcher* [1979], we generalize *Frank* [1966]'s method for calculating strain rates in triangles to strain rate estimations using many

angle measurements. The shear strain rates are plotted in Figure 7. The vertical bars show the 2σ errors and the horizontal bars denote the time over which the strain rate is averaged. The average shear strain rate during each time period is obtained by differencing angle measurements at the beginning and of the time period. The number of angle measurements used for each calculation ranges from 24 to 223. We omitted calculations that span the 1952 Kern County earthquake just north of the Mojave region and the 1971 San Fernando earthquake to minimize the influence of sources of deformation distinct from the San Andreas fault.

GPS time-series of postseismic displacements following the 1992 Landers earthquake are also plotted in Figure 7. We show only the four sites located farthest from the fault, although we used time-series data from nine sites in our inversions. We disregarded measurements during the first two years after the earthquake to avoid rapid velocities apparently associated with nonlinear flow in the upper mantle (e.g., *Freed and Bürgmann* [2004]) or afterslip (e.g., *Shen* et al. [1994], *Savage and Svarc* [1997]).

Probabilities on the timing of paleo-earthquakes on the Mojave segment of the San Andreas fault are shown in Figure 2. *Hilley and Young* [2006] calculated the timing probability distributions using published data on timing and time-separation of events from paleoseismic excavation sites and a Bayesian statistical method implementing a robust Markov-Chain Monte Carlo solution. In this study we focus on the timing probabilities for the Wrightwood site. *Hilley and Young* [2006] presented two solutions for the Wrightwood timings. The solution in Figure 2A uses all available timing constraints including radiocarbon ages and inferred rates of accumulation of peat. The more conservative solution in Figure 2B does not use the inferred peat accumulation rates.

6 Layered viscoelastic structure

To estimate lithosphere viscosity structure in the Mojave region, we build an earthquake cycle model incorporating multiple viscoelastic layers. In this section we discuss the construction of this model and illustrate the influence of layered viscoelastic structure on predicted interseismic surface velocities.

6.1 Model construction

We construct an earthquake cycle model consisting of an infinitely long strike-slip fault in an elastic crust overlying two Maxwell viscoelastic layers and a Maxwell viscoelastic half-space. The viscoelastic regions represent the lower crust, uppermost mantle, and upper mantle (Figure 3). The one-dimensional analog of a Maxwell viscoelastic solid is a spring connected to a dashpot, which is a plunger in a cylinder filled with a Newtonian viscous fluid ($n = 1$, equation 1). The multi-layer model is an extension of the earthquake cycle model concept introduce by *Savage and Prescott* [1978] in which the far-field steady velocity field is obtained by summing an infinite sequence of earthquakes on the fault. In the Savage-Prescott model, a fault is embedded in an elastic plate overlying a Maxwell viscoelastic half-space with uniform viscosity. Earthquakes are modeled as sudden uniform dislocations on a vertical fault. Earthquakes are imposed at a regular recurrence

interval and a steady far-field velocity is achieved after an infinite sequence of periodic earthquakes. *Meade and Hager* [2004] elaborated on this model to allow for clusters of periodic earthquakes, and *Hetland and Hager* [2005] extended the Savage-Prescott model to a general linear viscoelastic rheology. Our model differs from these earthquake cycle models in that we model a layered viscoelastic lower crust and mantle and non-periodic earthquake sequences.

We obtain the solution for a single earthquake in an elastic layer overlying two viscoelastic layers and a viscoelastic half-space with the propagator matrix method (e.g., *Pollitz* [1997]). Because the theory is linear, we can sum the solutions for the single earthquake to obtain the solution for a sequence of earthquakes. The steady far-field velocity is achieved by summing an infinite sequence of earthquakes. We obviously cannot specify the timing and slip for all earthquakes in the infinite sequence, so we break the sequence into a finite sequence extending from some time, t_0, before present to the present, and an infinite sequence extending from time $-\infty$ to time t_0. The earthquakes in the infinite sequence are assumed to have uniform slip and recurrence intervals. The slip and recurrence time is allowed to vary in the finite sequence. The solution for the infinite sequence is in the form of a convergent geometric series that has a closed form. The solution to this model is quasi-analytical and is therefore numerically efficient and amenable to inversion. The only numerical step in the solution is an inverse Fourier transform from wave-number space to physical space, and this is computed efficiently using the Fast Fourier Transform.

6.2 Surface velocity profiles

Figure 4 shows interseismic velocity profiles at four different times for a regular sequence of earthquakes with recurrence time of 200 years for the illustrated lithosphere structure. In each model, the viscosity is varied in the lower crust, uppermost mantle, and upper mantle. For reference, the velocity profiles predicted by the Savage-Prescott model are shown. The parameters in the Savage-Prescott models are the same as in the multi-layer models except the uniform viscosity is set to the upper mantle viscosity of the multi-layer model.

Figure 4B illustrates the effect of a relatively high viscosity lower crust and uppermost mantle overlying a lower viscosity mantle. The relatively high viscosity lower crust and uppermost mantle localizes the deformation near the fault with relatively steady shear strain rate within 50 km of the fault. The localized deformation occurs as a result of the low rate of diffusion of displacements away from the fault due to the high viscosity lower crust. The sustained localized flow below the fault generates localized deformation in the elastic crust. The low viscosity mantle allows the long wavelengths of elastic flexure to relax quickly. The effect is similar to flexure of an elastic plate loaded under shear and then cracked part way through the plate at the top. The cracked plate partly releases the load, but the plate below the crack supports some of the load and localizes deformation near the bottom tip of the crack.

Figure 4C shows interseismic velocities for a model similar to the the previous model, but including a lower viscosity lower crust. The velocity profiles are somewhat less localized near the fault than in Figure 4B, but the general pattern is quite similar.

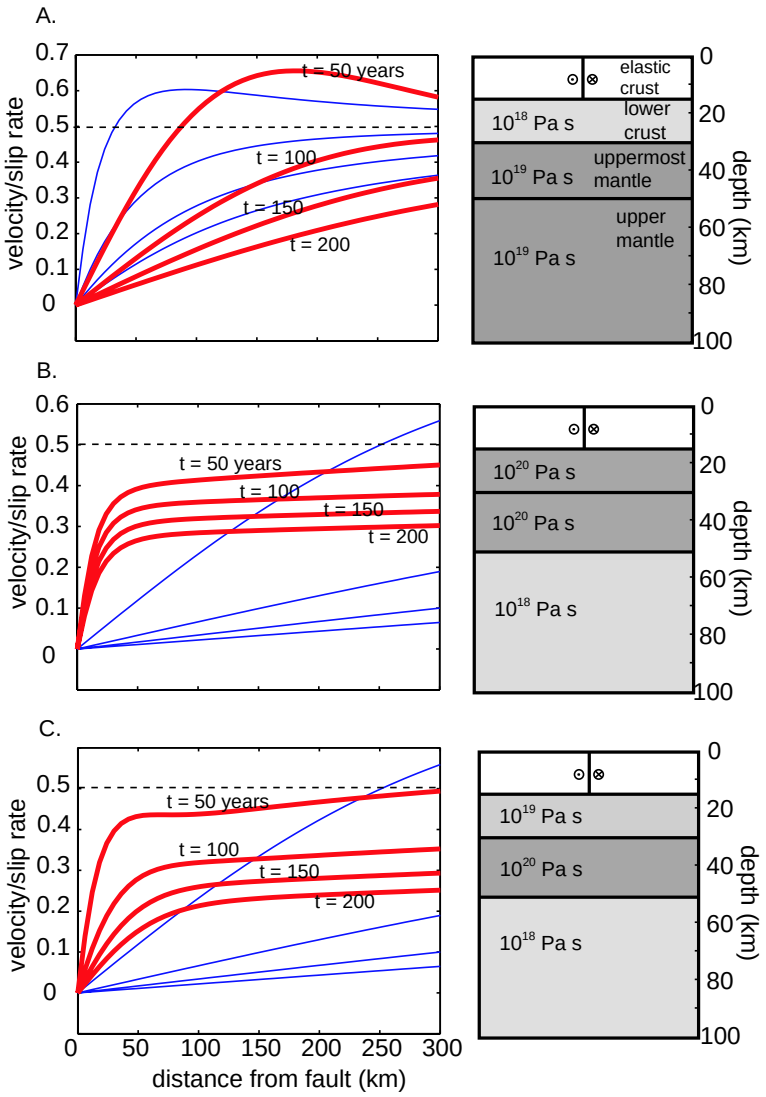

Figure 4: Illustration of effect of viscoelastic layering on surface velocity profiles. Heavy curves are velocities from the layered model and thin curves are velocities assuming a homogeneous viscosity half-space with viscosity equal to the upper mantle viscosity in the layered model. Viscosity structure assumed for each model is illustrated to the right of the velocity profiles.

A notable feature of of each of these models is that the velocities 300 km from the fault are significantly lower than the long-term plate velocities. The *Savage and Burford* [1973] buried elastic dislocation model would reproduce the velocities in Figure 4 with a lower slip rate, suggesting inversions of geodetic data for slip rates using elastic block models might underestimate the true fault slip rate.

7 Mojave model

We model the geodetic data in the Mojave region of the San Andreas fault system with the multilayer episodic earthquake cycle model discussed above (Figure 3). The timing of past earthquakes is constrained by paleoseismic data (Figure 2). We take t_0, the beginning of the non-periodic earthquake sequence, to be event EQ5 recorded at the Wrightwood site, about 1000 A.D. (Figure 2). Offsets and timing of earlier events are not resolved by our model.

The sensitivity of surface velocities to the timing and magnitude of past earthquakes is illustrated in Figure 5. We compare a reference surface velocity profile with velocity profiles generated with a random distribution of slip magnitude and timing of past earthquakes. The reference model has the rheological structure illustrated in Figure 5 with event times of the last seven earthquakes taken from the peak of the probability distributions for Wrightwood in Figure 2A, and coseismic slip of 4.3 m for each of these most recent events (which corresponds to 30 mm/yr average slip rate). Before event EQ5, it is assumed that earthquakes occur every 200 years with slip rate of 30 mm/yr. We then randomize the slip magnitude and timing of the seven most recent earthquakes by varying the timing within ± 50 years of the reference model and slip magnitude within ± 5 m of the reference model. The current surface velocities (year 2001) from the randomized models are subtracted from the reference surface velocities. The upper and lower bounds on the distribution of the differenced velocities are shown in Figure 5. We show three different results: randomized slip and timing for 1) the 1812 and 1857 earthquakes only, 2) earthquakes 1-5 only, and 3) earthquakes 6-11 only (numbering shown in Figure 2). Also plotted are the 2σ error bars for each of the GPS measurements as a function of distance from the San Andreas fault. We see that the surface velocities are most sensitive to slip and timing for the 1812 and 1857 earthquakes. The surface velocities within 100 km of the fault are sensitive to the timing and slip for earthquakes 1-5. However, only the long-wavelength component of the velocity profile is sensitive to timing and slip for earthquakes 6-11 and the variation is completely within the 2σ error. Clearly, the model and GPS data will not resolve slip and timing of the older events in the paleoseismic record and will only marginally resolve events EQ1-5.

We model the major faults in the Mojave region as infinitely long, parallel strike-slip faults, although in reality the faults are neither infinitely long nor parallel. We feel this is an adequate approximation to get first order estimates of lithosphere viscosity structure and fault slip rates. Three-dimensional models are the topic of current research and a future paper. We project GPS data within the dashed lines in Figure 1 onto a profile perpendicular to the trend of the Mojave segment of the San Andreas fault. The velocity profile is plotted in Figure 7. A line of GPS data across the Homestead and Emerson

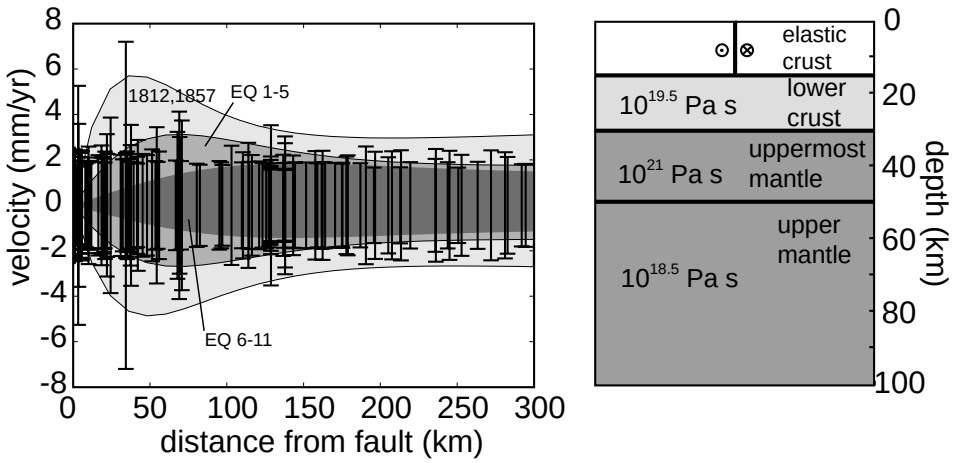

Figure 5: Illustration of sensitivity of model to timing and size of past earthquakes. Extent of shaded regions shows the maximum variation in surface velocities for a range of slip magnitudes and recurrence times for past earthquakes as discussed in the text. Earthquake numbering is defined in Figure 2. 2σ error bars for the GPS data are plotted as a function of distance from the fault. Illustration of the assumed viscosity structure to the right.

Valley faults that ruptured in the 1992 Landers earthquake is also projected onto a profile perpendicular to the faults.

Following *Meade and Hager* [2005], from west to east we model the Hosgri fault, San Gabriel fault, San Andreas fault and two faults in the eastern California shear zone (1). Although there a number of active fault strands in the eastern California shear zone, we model the entire zone with two parallel faults because we are not concerned with the details of deformation in the zone. Because we only have a detailed earthquake history along the San Andreas fault, this is the only fault for which we model viscoelastic cycle effects. The other faults are modeled as buried screw dislocations (*Savage and Burford* [1973]). We assign 5 mm/yr of slip on the San Gabriel fault following the results of *Meade and Hager* [2005], and we solve for the slip rate on the other faults. The locking depth for each of these buried dislocations is set at 15 km. This approximation using buried screw dislocations is valid because, for any velocity profile produced by our earthquake cycle model, there is a buried dislocation model that approximately reproduces the velocity profile (except during the earliest period of the cycle where local velocities can exceed the far-field velocity due to rapid relaxation of the coseismic load). The advantage is that there are fewer parameters to estimate in the buried dislocation model. The disadvantage is that we do not get an estimate of the slip rate and recurrence times because we do not have an established relationship that associates the buried dislocation solution to the corresponding similar viscoelastic cycle solution.

The post-Landers data is modeled with our multilayer viscoelastic model, but we impose a single earthquake rather than an infinite sequence of earthquakes.

8 Inversion scheme

To incorporate prior information on timing of past earthquakes, we formulate a Bayesian inversion scheme. Bayes' theorem provides the statistical basis for incorporating dis-

parate data sets into a single geophysical inversion. In Bayesian inversion, the posterior distribution, $\sigma(\mathbf{m})$, of the model parameters, $\mathbf{m}$, is a refinement of the prior distribution, $\rho_M(\mathbf{m})$,

$$\sigma(\mathbf{m}) = k \cdot \rho_M(\mathbf{m})\rho_D(\mathbf{m}) \tag{2}$$

where $\rho_D(\mathbf{m})$ is the distribution from the data only and k is a constant.

For this study, the parameters, $\mathbf{m}$, include slip rates on all the faults, timing of and slip during past earthquakes, elastic crust and uppermost mantle thickness, and viscosities of the lower crust, uppermost mantle, and upper mantle. The prior distribution on the model parameters, $\rho_M(\mathbf{m})$, is a quantitative estimate of the model parameters obtained independently of the geodetic data, as for example, the prior probability distributions on timing of past earthquakes (Figure 2).

Because the inversion is nonlinear and the prior distributions on earthquake times is a discrete distribution rather than a continuous function, we do not have a closed-form expression for the posterior distribution, $\sigma(\mathbf{m})$. We build the posterior distribution by sampling with a Montecarlo-Metropolis method (e.g., *Hilley* et al. [2005]) as explained briefly in *Johnson and Segall* [2004a]. This sampling technique requires running hundreds of thousands of forward models, which is practical given the the efficiency of our forward model.

We estimate the viscosity of the lower crust, uppermost mantle, and upper mantle as well as the thickness of the elastic crust and the depth to the top of the upper mantle. The the depth to the bottom of the lower crust is fixed to 30 km which is the average Moho depth in the Mojave region (e.g. *Zhu and Kanamori* [2000]). We estimate the timing of EQ 1-5 (shaded events in Figure 2), slip for EQ 1-4 and 1812 and 1857, and the average recurrence interval and long-term slip rate prior to EQ 5 (note that slip is not estimated for EQ 5 because it is the final earthquake in the infinite periodic sequence assigned uniform slip). The earthquakes leading up to EQ5 in Figure 2 are modeled as a periodic sequence and the recurrence time and slip rate are estimated in the inversion. All of the unknown parameters are listed in Table 2.

The priors assumed for all parameters are listed in Table 2 and plotted in Figure 6. The priors on timing of earthquakes are the paleoseismic probability density functions from the Wrightwood site constructed by *Hilley and Young* [2006] (Figure 2). We perform two inversions. One uses the Wrightwood probability distributions constructed using constraints from peat accumulation rates, and the other inversion uses the distributions that are not constrained by peat accumulation rates (order only). The prior distributions on coseismic slip are based loosely on studies by *Sieh* [1978] and *Salyards* et al. [9992]. We assumed box-car priors for the 1812 earthquake and EQ 1 because the paleoseismic data indicates that these earthquakes may not have ruptured the entire Mojave segment and therefore we did not want to put any prior weight on the slip magnitudes (Figure 2).

9 Results

Table 2 and Figures 6 and 7 summarize the inversion results using the prior probability distributions with full constraints for the Wrightwood site shown in Figure 2A. The long-term slip rate on the San Andreas fault is 24-32 mm/yr, in good agreement with the

25-35 mm/yr estimate from geologic data. Note that we provided no prior information directly on the long-term slip rate, so this is a result that derives entirely from the data and model. The prior distributions on slip magnitude in the five earthquakes before the 1857 event are broad and the inversion significantly refines the distribution only for the 1812 earthquake. The inversion shows that the 1812 earthquake was relatively small with only 1-3 meters of average slip. This may reflect the likely scenario that the 1812 earthquake ruptured only part of the Mojave segment. The inversion refines the estimate of slip in the 1857 earthquake as the 2-5.5 meters of slip is skewed toward the lower end of the prior distribution. The 2-5.5 meters of slip in the 1857 earthquake is quite similar to the estimated 2.5-5.5 meters of average slip in earthquakes prior to 1000 A.D. The 95% confidence interval on slip magnitudes during the four earthquakes between about 1000 A.D. and 1812 are larger than the average slip magnitude in the previous earthquakes because the slip magnitude is allowed to vary for these events and slip between sequential events is negatively correlated (i.e., lower than average slip in one event is correlated with higher than average slip in the following event). The inversion does not further refine the timing of earthquakes. Figure 6 shows that the prior and posterior distributions on timing are identical. This is also the case for the inversion using the order-only constraints for Wrightwood (Figure 2B). We do not show inversion results for the second inversion that uses the more conservative order-only constraints at Wrightwood since the results are nearly identical to the results using the prior with full constraints.

The 95% confidence intervals on lithosphere layer thicknesses and viscosities are plotted in Figure 3. It is quite amazing, given that there were no prior constraints on viscosity, that the viscosities are resolved to within 1-2 orders of magnitude in each layer. It is also quite interesting that the viscosity distribution with depth follows the general pattern expected from laboratory measurements; the average mantle viscosity is lower than the average upper mantle and lower crustal viscosities and the lower crustal viscosity is lower than the uppermost mantle viscosity.

10 Discussion

Our slip rate estimate of 24-32 mm/yr is higher than estimates from 3D elastic block models (*Becker* et al. [2004], *Meade and Hager* [2005]). However, our model differs from the 3D block models in that we are assuming infinitely long strike-slip faults and we model viscous flow below the elastic crust. To investigate whether the difference in slip rate estimates is due to different assumptions about rheology, we inverted the contemporary GPS data using a *Savage and Burford* [1973] buried fault model, which is the 2D equivalent to the 3D block models. This yields a slip rate of 17.5-21 mm/yr with locking depth of 18-24 km for the Mojave segment of the San Andreas fault (both 95% confidence limits). *Meade and Hager* [2005] report slip rate estimates of 13-15.5 mm/yr with locking depth of 15 km and *Becker* et al. [2004] report slip rates of 10-25 mm/yr with 15 km locking depth. Given the strong correlation between locking depth and slip rate and the fact that our locking depth estimate is greater than the 15 km assumed by *Meade and Hager* [2005] and *Becker* et al. [2004], it seems that the discrepancy between model slip rates can be largely accounted for by the different assumptions about rheology.

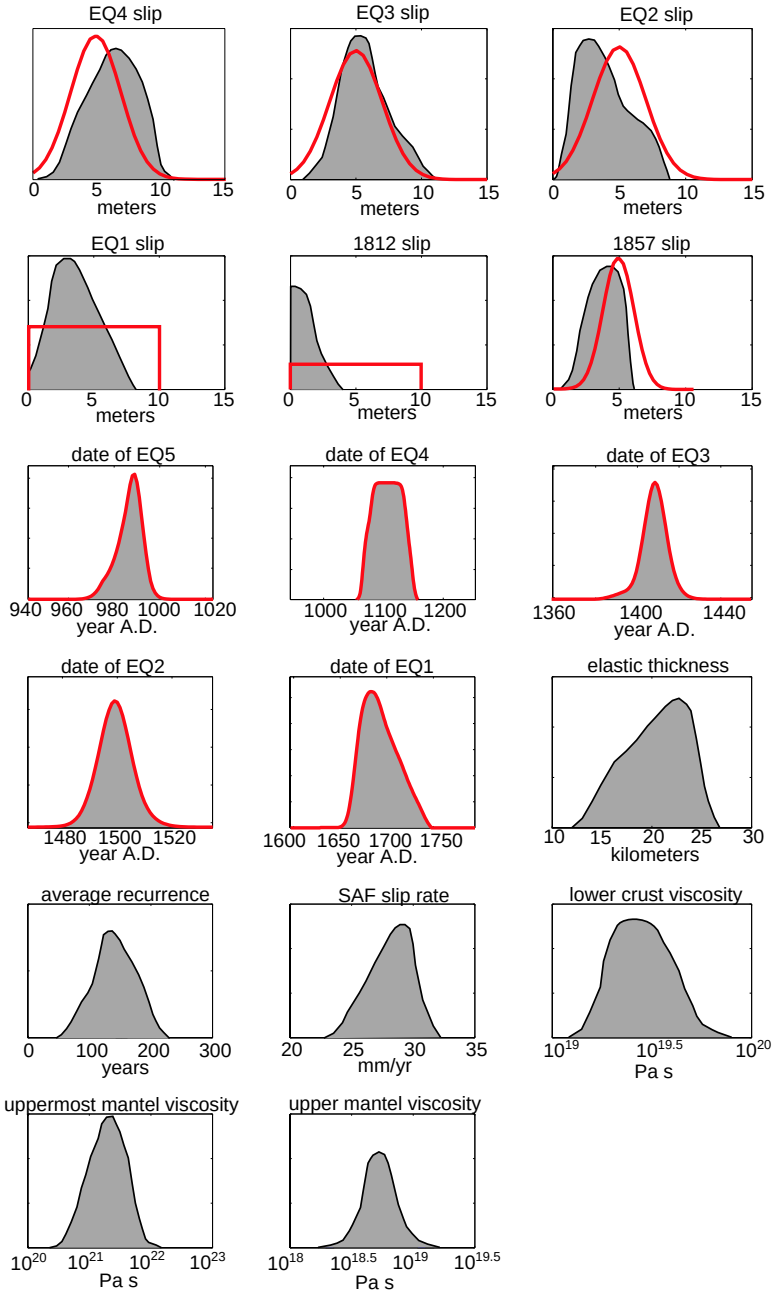

Figure 6: Posterior probability distributions from the Monte Carlo-Metropolis inversion. This inversion assumes the prior distributions on Wrightwood timing shown in Figure 2A. Red curves are prior distributions. Black curves and grey underlying areas show posterior distributions.

parameter	prior type	a priori	a posteriori (95%)
T (years)	u	0-∞	150-225
$\dot{s}_{SAF}$ (mm/yr)	u	0-∞	24-32
H_1 (km)	u	5-30	15-26
H_3 (km)	u	30-∞	52-66
η_1 (Pa)	u	0-∞	$10^{19} - 10^{20}$
η_2 (Pa)	u	0-∞	$10^{20} - 10^{22}$
η_3 (Pa)	u	0-∞	$10^{18} - 10^{19}$
s_{1857} (m)	g	3-7	2-5.5
s_{1812} (m)	u	0-10	1-3
s_1 (m)	u	0-10	1-6.5
s_2 (m)	g	1-9	1.5-7
s_3 (m)	g	1-9	3.5-9
s_4 (m)	g	1-9	3.5-9
s_{avg} (m)	u	0-∞	2.5-5.5
t_1 (yr)	p	1650-1730	1650-1730
t_2 (yr)	p	1480-1510	1480-1510
t_3 (yr)	p	1385-1420	1385-1420
t_4 (yr)	p	1050-1150	1050-1150
t_5 (yr)	p	970-1000	970-1000
$\dot{s}_{ECSZ}$ (mm/yr)	u	0-50	$10.5 - 13^*$
$\dot{s}_{HOS}$ (mm/yr)	u	0-50	$3.3 - 6^*$
$\dot{s}_{SG}$ (mm/yr)	fixed	5	-
$s_{Landers}$ (m)	u	0-10	4-8

Table 2: Second column lists the type of prior: u, uninformative (i.e., box-car distribution), g, Gaussian, p, paleoseismology. Third column gives upper and lower bounds on uninformative prior and 95% confidence intervals on Gaussian priors. Fourth column gives 95% confidence intervals on posterior distributions. T is average recurrence time before 900 A.D., $\dot{s}$ is average slip rate on each of the modeled faults. $H_{1,3}$ and η_{1-3} defined in Figure 3. s_i is coseismic slip for each earthquake and s_{avg} is the average coseismic slip magnitude before 900 A.D. t_i are the dates of earthquakes. SAF - San Andreas fault, ECSZ - Eastern California Shear Zone, HOS - Hosgri fault, SG - San Gregorio fault. *Buried dislocation result is not meaningful in context of the viscoelastic cycle model.

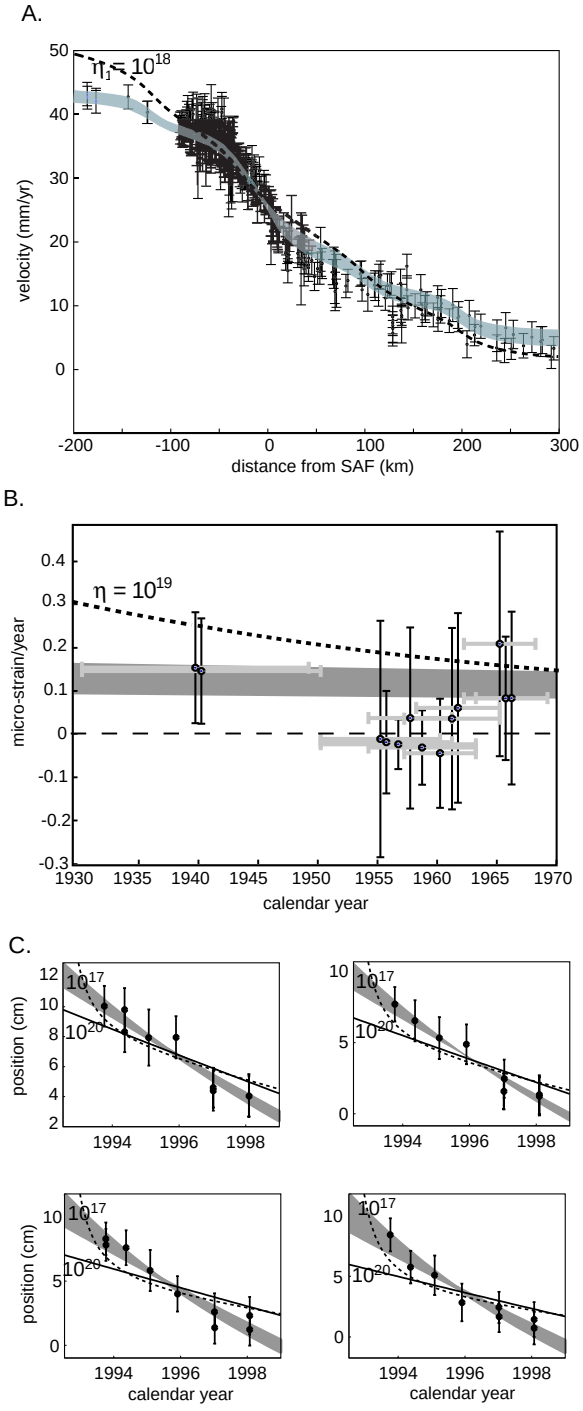

Figure 7: Fit to the data. Gray shading shows 95% confidence bounds on model predictions. A. Fit to contemporary GPS velocities. Dashed curve show best fit for viscous channel model with lower crustal viscosity fixed at 10^{18} Pa s. B. Fit to strain rate estimates from triangulation data. Vertical error bars are 2σ errors. Horizontal bars denote time period over which strain rate is averaged. Dashed curve shows best fit assuming uniform lower crust and mantle viscosity of 10^{19} Pa s. C. Fit to four post-Landers GPS time-series. Dashed and solid curves show results with upper mantle viscosity fixed to 10^{17} Pa s and 10^{20} Pa s.

It is yet unclear to what degree the 2D assumption affects the slip rate estimate. We are beginning to address this question with 3D viscoelastic earthquake cycle models.

The use of multiple data sets sampling different time periods of the earthquake cycle allows us to resolve the distribution of viscosity with depth. To demonstrate the importance of temporal data coverage on the viscosity estimates, we show the fit to the data for viscosities outside of the 95% confidence limits. Figure 7C illustrates that the constraints on mantle viscosity come largely from the post-Landers data. The dashed and solid curves show the modeled time-series assuming a mantle viscosity of 10^{17} Pa s and 10^{20} Pa s. The low viscosity mantle relaxes too quickly and the high viscosity mantle relaxes too slowly. The nearly steady shear strain rate across the San Andreas fault place constraints on the lower crust and uppermost mantle viscosities. The dashed curve in Figure 7B shows the best-fitting model with the lower crust and uppermost mantle viscosity fixed to 10^{19} Pa s. The shear strain rate is too high around 1940 and there is more variation in shear strain rate with time than the data suggests. A low viscosity channel in the lower crust is inconsistent with the data as illustrated in Figure 7A. The dashed curve in Figure 7A, which shows the best-fitting model when the viscosity of the lower crust is fixed to 10^{18} Pa s, does not fit the data. The post-Landers GPS data also places upper bounds on the lower crust and uppermost mantle viscosity. We found unbounded estimates of viscosity when the post-Landers data was not used in the inversion.

11 Publications resulting from this grant

Johnson, K.M., R. Bürgmann, and G. Hilley, 2006. Using geodetic and paleoseismic data with earthquake cycle models to image lithosphere viscosity structure and fault slip rates in the Mojave region of the San Andreas fault system. Abstract, 2006 UNAVCO Science Workshop, Denver, Colorado.

Johnson, K.M., G. Hilley, and R. Bürgmann, in prep. Fault slip rates and lithosphere viscosity structure in the Mojave region of the San Andreas fault system. To be submitted to JGR.

References

Becker, T. W., J. L. Hardebeck, and G. Anderson, Constraints on fault slip rates of the southern california plate boundary from gps velocity and stress inversions, *Geophysical Journal International*, *doi: 10.1111/j.1365-246X.2004.02528.x*, 2004.

Bills, B., D. Currey, and G. Marshall, Viscosity estimates for the crust and upper mantle from patterns of lacustrine shoreline deformation in the eastern great basin., *Journal of Geophysical Research*, *99*(B11), 22059–22086, 1994.

Bokelmann, G. and G. Beroza, Depth-dependent earthquake focal mechanism orientation: Evidence for a weak zone in the lower crust., *Journal of Geophysical Research*, *105*(B9), 21683 – 21695, 2000.

Deng, J., M. Gurnis, H. Kanamori, and E. Hauksson, Viscoelastic flow in the lower crust after the 1992 landers, california, earthquake., *Science*, *282*, 1689 – 1692, 1998.

Dixon, J. E., T. H. Dixon, D. R. Bell, and R. Malservisi, Lateral variation in upper mantle viscosity: role of water, *Earth and Planetary Science Letters*, *222*, 451–467, 2004.

Dixon, T., E. Norabuena, and L. Hotaling, Paleoseismology and global positioning system: Earthquake-cycle effects and geodetic versus geologic fault slip rates in the eastern california shear zone, *Geology*, *31*(1), 55–58, 2003.

Elsasser, W., Convection and stress propagation in the upper mantle, in S. Runcorn (ed.), *The application of modern physics to earth and planetary interiors*, pp. 223–245. New York: Wiley, 1969.

Frank, F. C., The deduction of earth strains from survey data., *Bulletin Seismological Society of America*, *56*, 35 – 42, 1966.

Freed, A. M. and R. Bürgmann, Evidence of power-law flow in the mojave desert mantle, *Nature*, *430*, 548–551, 2004.

Fumal, T. E., I. R. J. Weldon, G. P. Biasi, T. E. Dawson, G. G. Seitz, W. T. Frost, and D. P. Schwartz, Evidence for large earthquakes on the san andreas fault at the wrightwood, california, paleoseismic site: A.d. 500 to present., *Bulletin of the Seismological Society of America*, *92*(7), 2726 – 60, 2002.

Goes, S. and S. van der Lee, Termal structure of the north america uppermost mantle inferred from seismic tomography., *Journal of Geophysical Research*, *107*(B3), doi:10.1029/2000JB000049, 2002.

Hetland, E. A. and B. H. Hager, Postseismic and interseismic displacements near a strike-slip fault: A two-dimensional theory for general linear viscoelastic rheologies., *Journal of Geophysical Research*, *110*(B10401), doi:10.1029/2005JB003689, 2005.

Hilley, G. E. and J. J. Young, Determining event timing, recurrence, and correlation from paleoseismic excavation data along the central and southern san andreas fault, california, *Journal of Geophysical Research*, *in review*, 2006.

Hilley, G. E., R. Burgmann, P. Zhang, and P. Molnar, Bayesian inference of plastosphere viscosities near the kunlun fault, northern tibet, *Geophysical Research Letters*, *32*(L01302), doi:10.1029/2004GL0021658, 2005.

Johnson, K. and P. Segall, Viscoelastic earthquake cycle models with deep stress-driven creep along the san andreas fault system, *Journal Geophysical Research*, *109*(B10403), doi:10.1029/2004JB003096, 2004a.

Johnson, K. M. and P. Segall, Imaging the ramp-decollement geometry of the chelungpu fault using coseismic gps displacements from the 1999 chi-chi, taiwan earthquake, *Tectonophysics*, *378*(1-2), 123 – 139, 2004b.

Kaufman, P. and L. Royden, Lower crustal flow in an extensional setting: Constraints from the halloran hills region, eastern mojave desert, california., *Journal of Geophysical Research*, *99*(B8), 15723 – 15739, 1994.

Kaufmann, G. and F. Amelung, Reservoir-induced deformation and continental rheology in vicinity of lake meade, nevada., *Journal of Geophysical Research*, *105*, 16341–16358, 2000.

Kohlstedt, D., B. Evans, and S. Mackwell, Strength of the lithosphere: Constraints imposed by laboratory experiments., *Journal of Geophysical Research*, *100*, 17587–17602, 1995.

Liu, J., Y. Klinger, K. Sieh, and C. Rubin, Six similar sequential ruptures of the san andreas fault, carrizo plain, california., *Geology*, *32*(8), 649 – 652, 2004.

Meade, B. J. and B. H. Hager, Viscoelastic deformation for a clustered earthquake cycle., *Geoophysical Research Letters*, *31*(L10610), doi:10.1029/2004GL019643, 2004.

Meade, B. J. and B. H. Hager, Block models of present crustal motion in southern california constrained by gps measurements, *Journal of Geophysical Research*, *110*(B03403), doi:10.1029/2004JB003209, 2005.

NGS, Classical direction observations for ngs geodetic horizontal control stations in california, Technical report, NOAA, National Geodetic Survey, 2004.

Nishimura, T. and W. Thatcher, Rheology of the lithosphere inferred from postseismic uplift following the 1959 hebgen lake earthquake., *Journal of Geophysical Research*, *108*(B8), doi:10.1029/2002JB002191, 2003.

Pollitz, F., Transient rheology of the uppermost mantle beneath the mojave desert, california, *Earth and Planetary Science Letters*, *215*, 89–104, 2003.

Pollitz, F., G. Peltzer, and R. Bürgmann, Mobility of continental mantle: Evidence from postseismic geodetic observations following the 1992 landers earthquake, *Journal of Geophysical Research*, *105*, 8035–8054, 2000.

Pollitz, F., C. Wicks, and W. Thatcher, Mantle flow beneath a continental strike-slip fault: postseismic deformation after the 1999 hector mine earthquake, *Science*, *293*, 1814–1818, 2001.

Pollitz, F. F., Gravitational viscoelastic postseismic relaxation on a layered spherical earth, *Journal of Geophysical Research*, *102*(B8), 17921 – 17941, 1997.

Salyards, S. L., K. E. Sieh, and J. L. Kirschvink, Paleomagnetic measurement of nonbrittle coseismic deformation across the san andreas fault at pallett creek., *Journal of Geophysical Research*, *97*(B9), 12457 – 12470, 19992.

Savage, J. and R. Burford, Geodetic determination of relative plate motion in central California, *Journal of Geophysical Research*, *78*, 832–845, 1973.

Savage, J. and W. Prescott, Asthenosphere readjustment and the earthquake cycle, *Journal of Geophysical Research*, *83*, 3369–3376, 1978.

Savage, J. and J. Svarc, Postseismic deformation associated with the 1992 mw=7.3 landers earthquake, southern california., *Journal Geophysical Research*, *102*, 7565–7577, 1997.

Segall, P., Integrating geologic and geodetic estimates of slip rate on the san andreas fault system, *International Geology Review*, *44*, 62–82, 2002.

Shen, Z.-K., D. D. Jackson, Y. Feng, M. Cline, M. Kim, P. Fang, and Y. Bock, Postseismic deformation following the 1992 landers earthquake, *Seismological Society of America Bulletin*, *84*, 780–791, 1994.

Sieh, K. and R. Jahns, Holocene activity of the san andreas fault at wallace creek, california, *Geological Society of America Bulletin*, *95*, 883–896, 1984.

Sieh, K. E., Slip along the san andreas fault associated with the great 1857 earthquake, *Bulletin Seismological Society of America*, *68*, 1421 – 1428, 1978.

Thatcher, W., Horizontal crustal deformation from historic geodetic measurements in southern california, *Journal of Geophysical Research*, *84*(B5), 2351 – 2370, 1979.

Weldon, R., T. Fumal, and G. Biasi, Wrightwood and the earthquake cycle: What a long recurrence record tells us about how faults work, *GSA Today*, *14*(9), doi:10.1130/1052–5173, 2004.

Zhu, L. and H. Kanamori, Moho depth variation in southern california from teleseismic receiver functions, *Journal Geophysical Research*, *105*(B2), 2969 – 2980, 2000.